Supplementary Materials

6-Bromo-2-hydroxypyridinate-bridged Paddlewheel-type Dirhodium Complex Isomers: Synthesis, Crystal Structures, electrochemical properties, and Structure-dependent Absorption Properties

Kozo Sato,[1] Natsumi Yano,[1,2] Yusuke Kataoka [1,*]

[1] Department of Chemistry, Graduate School of Natural Science and Technology, Shimane University, 1060, Nishikawatsu, Matsue, Shimane 690-8504, Japan.

[2] Special Course in Science and Engineering, Graduate School of Natural Science and Technology, Shimane University, 1060, Nishikawatsu, Matsue, Shimane 690-8504, Japan.

Contents

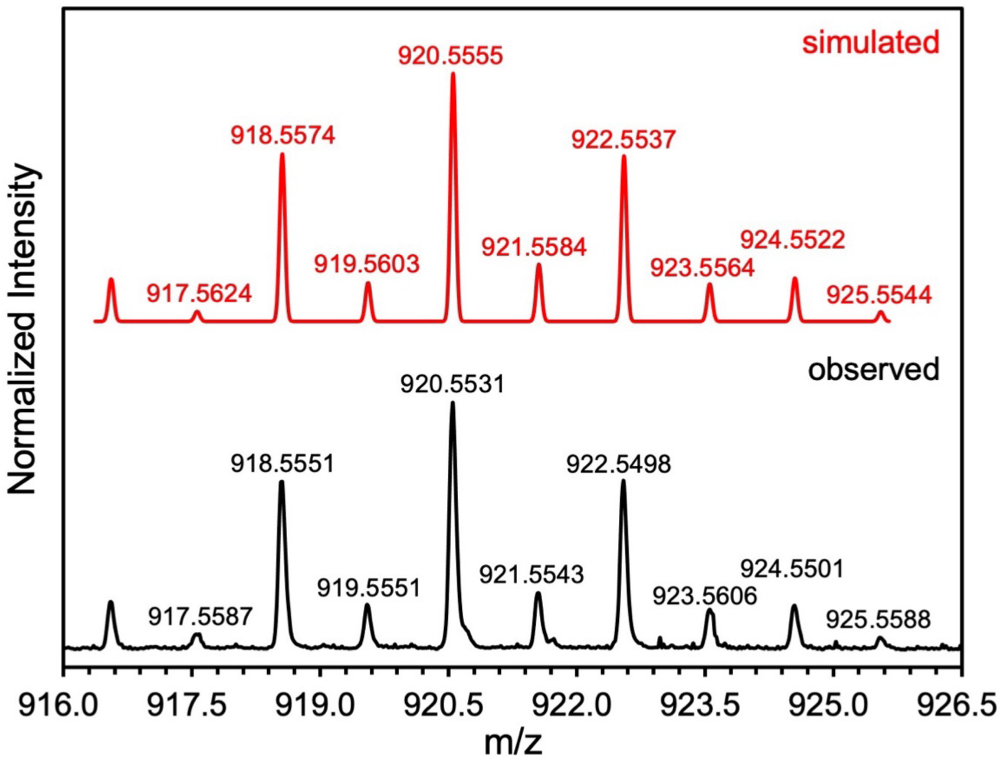

Figure S1. Observed and simulated ESI-MS spectra of *trans-2,2*-[Rh_2(bhp)$_4$].

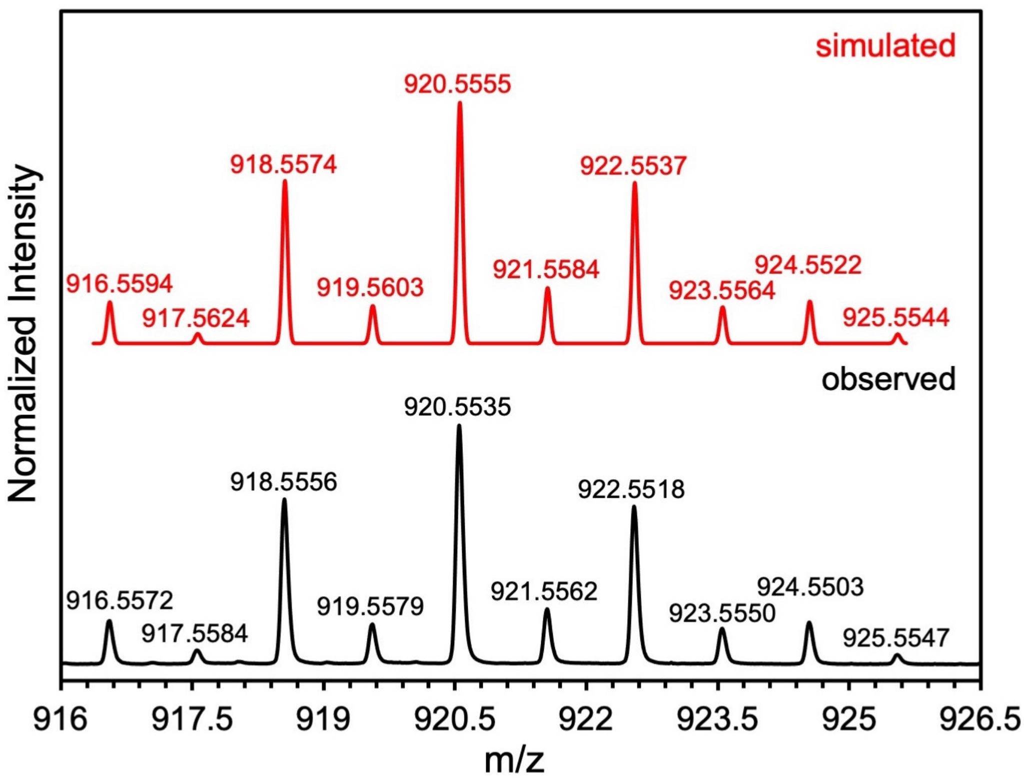

Figure S2. Observed and simulated ESI-MS spectra of *3,1*-[Rh_2(bhp)$_4$].

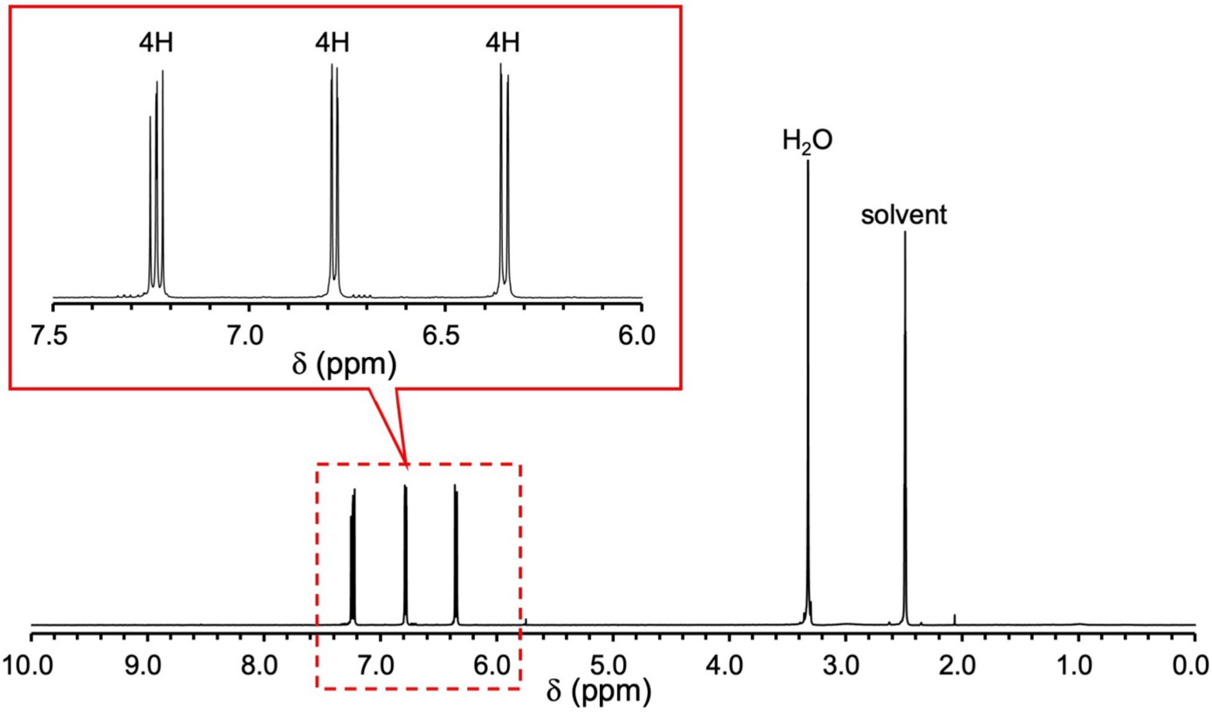

Figure S3. [1]H NMR spectrum of *trans-2,2*-[Rh_2(bhp)$_4$] in DMSO-d_6.

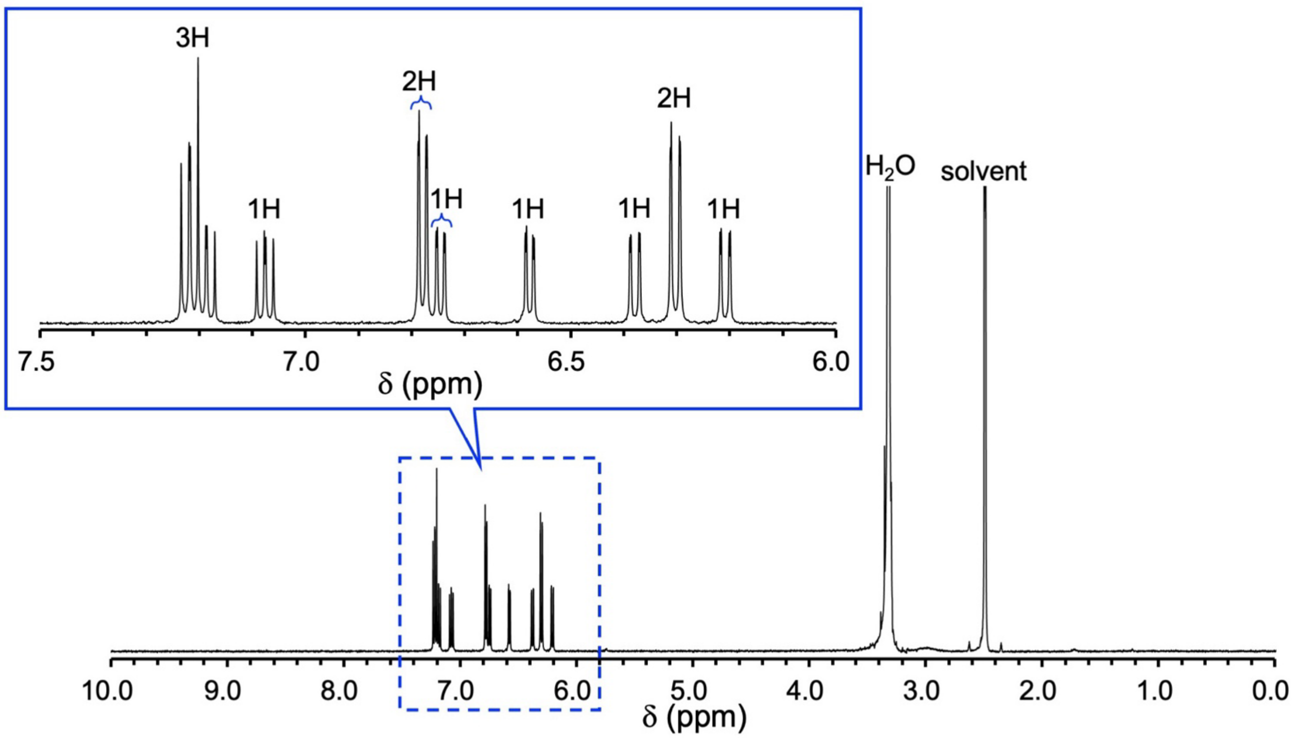

Figure S4. [1]H NMR spectrum of *3,1*-[Rh_2(bhp)$_4$] in DMSO-d_6.

Table S1. Selected bond lengths (Å) and angles (°) of *trans-2,2*-[$Rh_2(bhp)_4$].

bond lengths (Å)			
Rh1-Rh2	2.3902(4)	C1-N1	1.297(5)
Rh1-O2	2.029(3)	C1-O1	1.365(5)
Rh1-O4	2.023(3)	C6-O2	1.298(5)
Rh1-N1	2.048(3)	C6-N2	1.362(5)
Rh1-O3	2.040(3)	C11-N3	1.365(5)
Rh2-O1	2.007(3)	C11-O3	1.300(5)
Rh2-O3	2.023(3)	C16-N4	1.363(5)
Rh2-N2	2.047(4)	C16-O4	1.296(5)
Rh2-N4	2.058(4)		
bond angles (°)			
Rh1-Rh2-O1	90.66(8)	Rh2-Rh1-O2	90.78(8)
Rh1-Rh2-O3	90.23(8)	Rh2-Rh1-O4	89.82(8)
Rh1-Rh2-N2	86.97(10)	Rh2-Rh1-N1	87.33(9)
Rh1-Rh2-N4	87.91(10)	Rh2-Rh1-N3	87.55(9)

Table S2. Selected bond lengths (Å) and angles (°) of *3,1*-[$Rh_2(bhp)_4$(DMF)].

bond lengths (Å)			
Rh1-Rh2	2.3726(11)	Rh1-O5	2.173(7)
Rh1-O1	2.026(7)	C1-N1	1.385(12)
Rh1-O2	2.023(7)	C1-O1	1.296(13)
Rh1-O3	2.027(6)	C6-O2	1.285(13)
Rh1-N4	2.030(8)	C6-N2	1.362(14)
Rh2-N1	2.054(8)	C11-N3	1.360(14)
Rh2-N2	2.070(8)	C11-O3	1.275(12)
Rh2-N3	2.043(9)	C16-N4	1.379(13)
Rh2-O4	2.048(6)	C16-O4	1.285(13)
bond angles (°)			
Rh1-Rh2-N1	86.8(2)	Rh2-Rh1-O1	89.1(2)
Rh1-Rh2-N2	86.2(2)	Rh2-Rh1-O2	87.1(2)
Rh1-Rh2-N3	85.8(2)	Rh2-Rh1-O3	87.3(2)
Rh1-Rh2-O4	85.9(2)	Rh2-Rh1-N4	88.0(2)
Rh2-Rh1-O5	173.5(2)		

Table S3. Selected bond lengths (Å) and angles (°) of *3,1*-$[Rh_2(bhp)_4]_2$.

bond lengths (Å)			
Rh1-Rh2	2.3704(4)	Rh3-Rh4	2.3707(5)
Rh1-O1	2.031(2)	Rh3-O5	2.020(2)
Rh1-O2	2.015(3)	Rh3-O6	2.014(3)
Rh1-O3	2.032(2)	Rh3-O7	2.020(2)
Rh1-N4	2.052(3)	Rh3-N8	2.055(4)
Rh2-N1	2.064(3)	Rh4-N5	2.066(3)
Rh2-N2	2.058(3)	Rh4-N6	2.064(4)
Rh2-N3	2.037(3)	Rh4-N7	2.054(3)
Rh2-O4	2.021(3)	Rh4-O8	2.019(3)
Rh1-O5	2.336(3)	Rh3-O1	2.250(3)
C1-N1	1.366(5)	C21-N5	1.375(5)
C1-O1	1.308(5)	C21-O5	1.293(5)
C6-O2	1.287(5)	C26-O6	1.287(5)
C6-N2	1.377(5)	C26-N6	1.378(6)
C11-N3	1.376(5)	C31-N7	1.376(6)
C11-O3	1.297(5)	C31-O7	1.286(5)
C16-N4	1.380(5)	C36-N8	1.379(5)
C16-O4	1.296(5)	C36-O8	1.279(5)
bond angles (°)			
Rh1-Rh2-N1	86.17(9)	Rh3-Rh4-N5	85.83(10)
Rh1-Rh2-N2	87.24(9)	Rh3-Rh4-N6	87.32(10)
Rh1-Rh2-N3	87.03(10)	Rh3-Rh4-N7	86.58(10)
Rh1-Rh2-O4	87.63(8)	Rh3-Rh4-O8	86.61(8)
Rh2-Rh1-O1	88.94(8)	Rh4-Rh3-O5	89.36(8)
Rh2-Rh1-O2	87.41(8)	Rh4-Rh3-O6	86.46(8)
Rh2-Rh1-O3	87.11(8)	Rh4-Rh3-O7	87.17(8)
Rh2-Rh1-N4	86.84(10)	Rh4-Rh3-N8	86.97(10)
Rh2-Rh1-O5	160.57(7)	Rh4-Rh3-O1	164.17(7)

Table S4. Averaged bond lengths (Å) of optimized geometries of $[Rh_2(bhp)_4]$ isomers.

Isomer	*4,0*-form		*3,1*-form		*cis*-*2,2*-form		*trans*-*2,2*-form	
spin state	singlet	triplet	singlet	triplet	singlet	triplet	singlet	triplet
Rh-Rh	2.390	2.504	2.407	2.504	2.413	2.517	2.414	2.498
Rh-O	2.031	2.011	2.042	2.029	2.040	2.029	2.042	2.032
Rh-N	2.135	2.150	2.101	2.115	2.097	2.094	2.097	2.106

Table S5. TDDFT results of *trans-2,2*-$[Rh_2(bhp)_4]$ in CH_2Cl_2.

Excitation States	Wavelength (nm)	Oscillator strength	Excitation characters
S_2	762.7	0.0026	H-3[π*(Rh_2)]→L[σ*(Rh_2)] (74%), H-4[delocalized MO]→L[σ*(Rh_2)] (13%)
S_3	759.8	0.0043	H-2[π*(Rh_2)]→L[σ*(Rh_2)] (58%), H-5[delocalized MO]→L[σ*(Rh_2)] (29%)
S_4	533.7	0.0001	H-1[π(bhp)]→L[σ*(Rh_2)] (91%)
S_5	483.4	0.0002	H[δ*(Rh_2)]→L+1[*anti-bonding*-dx^2-y^2(Rh_2)] (75%)
S_6	460.8	0.0005	H-4[delocalized MO]→L[σ*(Rh_2)] (81%), H-3[π*(Rh_2)]→L[σ*(Rh_2)] (14%)
S_7	460.0	0.0006	H-5[delocalized MO]→L[σ*(Rh_2)] (63%), H-2[π*(Rh_2)]→L[σ*(Rh_2)] (32%)
S_9	406.4	0.0004	H-7[δ(Rh_2)]→L[σ*(Rh_2)] (88%)
S_{10}	404.0	0.0003	H-8[δ(Rh_2)]→L[σ*(Rh_2)] (62%)

Table S6. TDDFT results of *3,1*-[Rh_2(bhp)$_4$] in CH_2Cl_2.

Excitation States	Wavelength (nm)	Oscillator strength	Excitation characters
S_1	819.7	0.0001	H[δ*(Rh_2)]→L[σ*(Rh_2)] (95%)
S_2	780.3	0.0030	H-2[delocalized MO]→L[σ*(Rh_2)] (48%), H-5[π*(Rh_2)]→L[σ*(Rh_2)] (24%), H-1[delocalized MO]→L[σ*(Rh_2)] (13%)
S_3	750.8	0.0036	H-4[π*(Rh_2)]→L[σ*(Rh_2)] (67%), H-1[π(bhp)]→L[σ*(Rh_2)] (14%), H-5[π*(Rh_2)]→L[σ*(Rh_2)] (13%)
S_4	505.8	0.0002	H-3[delocalized MO]→L[σ*(Rh_2)] (52%), H-1[delocalized MO]→L[σ*(Rh_2)] (20%), H-2[delocalized MO]→L[σ*(Rh_2)] (11%)
S_6	484.9	0.0008	H[δ*(Rh_2)]→L[σ*(Rh_2)] (39%), H-1[delocalized MO]→L[σ*(Rh_2)] (22%)
S_7	469.8	0.0011	H-5[π*(Rh_2)]→L[σ*(Rh_2)] (51%), H-2[delocalized MO]→L[σ*(Rh_2)] (26%)
S_8	440.6	0.0001	H[δ*(Rh_2)]→L+4[delocalized MO] (23%), H[δ*(Rh_2)]→L+5[delocalized MO] (14%), H[δ*(Rh_2)]→L+6[*bonding*-dx^2-y^2(Rh_2)/π*(bhp)] (20%)
S_9	424.4	0.0004	H-7[δ(Rh_2)]→L[σ*(Rh_2)] (39%), H-6[d(Rh_2)]→L[σ*(Rh_2)] (30%), H-8[π(Rh_2)]→L[σ*(Rh_2)] (14%)
S_{10}	404.8	0.0003	H-8[π(Rh_2)]→L[σ*(Rh_2)] (34%), H-4[π*(Rh_2)]→L+1[*anti-bonding*-dx^2-y^2(Rh_2)] (12%), H-6[d(Rh_2)]→L[σ*(Rh_2)] (11%)

Table S7. TDDFT results of *3,1*-[Rh_2(bhp)$_4$] in DMF.

Excitation States	Wavelength (nm)	Oscillator strength	Excitation characters
S_1	607.7	0.0016	H-1[π*(Rh_2)]→L[σ*(Rh_2)] (78%)
S_2	602.5	0.0039	H-2[π*(Rh_2)]→L[σ*(Rh_2)] (82%)
S_3	555.5	0.0001	H[δ*(Rh_2)]→L[σ*(Rh_2)] (95%)
S_4	497.9	0.0005	H[δ*(Rh_2)]→L+1[*anti-bonding*-dx^2-y^2(Rh_2)] (63%), H[δ*(Rh_2)]→L+6[d(Rh_2)/π(bhp)] (12%)
S_5	444.8	0.0001	H[δ*(Rh_2)]→L+2[delocalized MO] (26%), H[δ*(Rh_2)]→L+5[*bonding*-dx^2-y^2(Rh_2)/π*(bhp)] (16%), H-6[π(bhp)/d(Rh_2)]→L+1[*anti-bonding*-dx^2-y^2(Rh_2)] (10%)
S_6	423.3	0.0003	H-1[π*(Rh_2)]→L+1[*anti-bonding*-dx^2-y^2(Rh_2)] (44%)
S_8	411.7	0.0009	H-3[π(bhp)/d(Rh_2)]→L[σ*(Rh_2)] (46%), H-1[π*(Rh_2)]→L+1[*anti-bonding*-dx^2-y^2(Rh_2)] (12%), H-2[π*(Rh_2)]→L+1[*anti-bonding*-dx^2-y^2(Rh_2)] (11%)

Table S8. TDDFT results of *3,1*-[Rh_2(bhp)$_4$] in gas phase.

Excitation States	Wavelength (nm)	Oscillator strength	Excitation characters
S_1	665.7	0.0064	H-3[π*(Rh_2)]→L[σ*(Rh_2)] (37%), H-1[δ*(Rh_2)]→L[σ*(Rh_2)] (12%), H-8[d(Rh_2)/π(bhp)]→L+1[σ*(Rh_2)] (10%), H-6[π*(Rh_2)]→L+1[σ*(Rh_2)] (10%), H-4[π*(Rh_2)]→L+1[σ*(Rh_2)] (10%)
S_2	663.0	0.0009	H-6[π*(Rh_2)]→L[σ*(Rh_2)] (24%), H-3[π*(Rh_2)]→L+1[σ*(Rh_2)] (24%), H-8[d(Rh_2)/π(bhp)]→L[σ*(Rh_2)] (16%)
S_3	649.7	0.0014	H-4[π*(Rh_2)]→L[σ*(Rh_2)] (31%), H-9[π*(Rh_2)]→L+1[σ*(Rh_2)] (18%), H-6[π*(Rh_2)]→L[σ*(Rh_2)] (16%), H[δ*(Rh_2)]→L[σ*(Rh_2)] (10%)
S_4	641.7	0.0007	H-9[π*(Rh_2)]→L[σ*(Rh_2)] (27%), H-4[π*(Rh_2)]→L+1[σ*(Rh_2)] (24%), H-6[π*(Rh_2)]→L+1[σ*(Rh_2)] (13%)
S_5	630.2	0.0004	H[δ*(Rh_2)]→L[σ*(Rh_2)] (49%), H-1[δ*(Rh_2)]→L+1[σ*(Rh_2)] (34%)
S_6	628.6	0.0001	H-1[δ*(Rh_2)]→L[σ*(Rh_2)] (51%), H[δ*(Rh_2)]→L+1[σ*(Rh_2)] (32%)
S_7	504.0	0.0019	H-1[δ*(Rh_2)]→L+2[*anti-bonding*-dx^2-y^2(Rh_2)] (19%), H[δ*(Rh_2)]→L+1[σ*(Rh_2)] (17%), H[δ*(Rh_2)]→L+3[*anti-bonding*-dx^2-y^2(Rh_2)] (16%)
S_8	503.6	0.0003	H-1[δ*(Rh_2)]→L+3[*anti-bonding*-dx^2-y^2(Rh_2)] (19%), H-1[δ*(Rh_2)]→L+1[σ*(Rh_2)] (17%) H[δ*(Rh_2)]→L+2[*anti-bonding*-dx^2-y^2(Rh_2)] (18%)
S_{10}	457.4	0.0016	H[δ*(Rh_2)]→L+1[σ*(Rh_2)] (35%), H-1[δ*(Rh_2)]→L[σ*(Rh_2)] (21%), H[δ*(Rh_2)]→L+3[*anti-bonding*-dx^2-y^2(Rh_2)] (11%)
S_{11}	456.7	0.0003	H-1[δ*(Rh_2)]→L+1[σ*(Rh_2)] (27%), H[δ*(Rh_2)]→L[σ*(Rh_2)] (14%), H-2[π(bhp)]→L[σ*(Rh_2)] (11%)
S_{12}	454.6	0.0002	H-5[π(bhp)]→L[σ*(Rh_2)] (35%), H-2[π(bhp)]→L+1[σ*(Rh_2)] (34%), H-7[π(bhp)]→L[σ*(Rh_2)] (11%)
S_{15}	429.6	0.0015	H-3[π*(Rh_2)]→L[σ*(Rh_2)] (38%), H-4[π*(Rh_2)]→L+1[σ*(Rh_2)] (19%)
S_{17}	420.9	0.0027	H-9[π*(Rh_2)]→L[σ*(Rh_2)] (16%), H-8[d(Rh_2)/π(bhp)]→L+1[σ*(Rh_2)] (16%), H-7[π(bhp)]→L[σ*(Rh_2)] (15%)
S_{18}	420.6	0.0005	H-8[d(Rh_2)/π(bhp)]→L[σ*(Rh_2)] (22%), H-9[π*(Rh_2)]→L+1[σ*(Rh_2)] (14%)
S_{19}	408.7	0.004	H-11[d(Rh_2)/π(bhp)]→L[σ*(Rh_2)] (16%), H-4[π*(Rh_2)]→L+3[*anti-bonding*-dx^2-y^2(Rh_2)] (15%), H-3[π*(Rh_2)]→L+2[*anti-bonding*-dx^2-y^2(Rh_2)] (13%)
S_{21}	404.7	0.0023	H-6[π*(Rh_2)]→L+1[σ*(Rh_2)] (22%), H-9[π*(Rh_2)]→L[σ*(Rh_2)] (13%), H-6[π*(Rh_2)]→L+3[*anti-bonding*-dx^2-y^2(Rh_2)] (11%)
S_{22}	401.3	0.0002	H-10[d(Rh_2)/π(bhp)]→L[σ*(Rh_2)] (17%), H-4[π*(Rh_2)]→L+2[*anti-bonding*-dx^2-y^2(Rh_2)] (14%), H-3[π*(Rh_2)]→L+3[*anti-bonding*-dx^2-y^2(Rh_2)] (12%), H-3[π*(Rh_2)]→L+1[σ*(Rh_2)] (10%)